Published in final edited form as:
Dev Biol. 2014 November 1; 395(1): 84–95. doi:10.1016/j.ydbio.2014.08.026.

Peripheral nervous system defects in a mouse model for peroxisomal biogenesis disorders

M. Gartz Hanson[1], **Veronica Fregoso**[2], **Justin D. Vrana**[3], **Chandra L. Tucker**[3], and **Lee A. Niswander**[1,2]

[1]Howard Hughes Medical Institute, Dept. of Pediatrics, University of Colorado School of Medicine and Children's Hospital Colorado, Aurora, CO 80045

[2]Graduate Program in Cell Biology, Stem Cells, and Development, University of Colorado School of Medicine and Children's Hospital Colorado, Aurora, CO 80045

[3]Dept. of Pharmacology University of Colorado School of Medicine and Children's Hospital Colorado, Aurora, CO 80045

Abstract

Peroxisome biogenesis disorders (PBD) are autosomal recessive disorders in humans characterized by skeletal, eye and brain abnormalities. Despite the fact that neurological deficits, including peripheral nervous system (PNS) defects, can be observed at birth in some PBD patients including those with *PEX10* mutations, the embryological basis of the PNS defects is unclear. Using a forward genetic screen, we identified a mouse model for *Pex10* deficiency that exhibits neurological abnormalities during fetal development. Homozygous *Pex10* mutant mouse embryos display biochemical abnormalities related to a PBD deficiency. During late embryogenesis, *Pex10* homozygous mutant mice experience progressive loss of movement and at birth they become cyanotic and die shortly thereafter. Homozygous *Pex10* mutant fetuses display decreased integrity of axons and synapses, over-extension of axons in the diaphragm and decreased Schwann cell numbers. Our neuropathological, molecular and electrophysiological studies provide new insights into the embryological basis of the PNS deficits in a PBD model. Our findings identify PEX10 function, and likely other PEX proteins, as an essential component of the spinal locomotor circuit.

Keywords

peroxisome; Acetylcholine receptor; neuromuscular junction; synapse formation; axon integrity

Corresponding author: M. Gartz Hanson; University of Colorado School of Medicine; Bldg. L18-12400E; 12801, E. 17th Ave., Aurora, CO 80045, martin.hanson@ucdenver.edu, Phone: 303 724-3797, FAX: 303 724-3792.

The authors declare that no conflict of interest exists.

Introduction

Clinically, peroxisome biogenesis disorders (PBD) are lethal congenital diseases with a spectrum of severity and progressiveness(Braverman et al., 2013; Steinberg et al., 2006). Infants born with Zellweger syndrome (ZS), the most severe disease within the spectrum of PBD, may show a lack of muscle tone and an inability to move, indicating an embryonic origin of the disorder (Wanders and Waterham, 2005, 2006). ZS is lethal within six months and is associated with impaired neuronal migration, abnormal brain development and severe degradation of the white matter. Patients with the PBD, neonatal adrenoleukodystrophy (NALD), display demyelination of white matter tracks in the brain and spinal cord, which results in progressive weakness and mortality within ten years(Steinberg et al., 2006). Ataxia, demyelination and loss of axon integrity are common in patients with peroxisomal dysfunction(Baes and Aubourg, 2009; Steinberg et al., 2006). A common cellular pathology of these diseases is the inability to generate functional peroxisomes to meet the metabolic demands of the cell.

Peroxisomes are single-membrane bound subcellular organelles present in all eukaryotic cells. Mammalian peroxisomes are involved in the breakdown of very long chain fatty acids (VLCFA), amino acids, and polyamines, decomposition of hydrogen peroxide, as well as the biosynthesis of plasmalogens, which are abundant in myelin, bile acids, and polyunsaturated fatty acids. Peroxisome enzyme content, number, and metabolic functions are determined by the cell type and species(Brown et al., 2008). Peroxisomal proteins called peroxins (PEX) control peroxisome assembly, fission, and shuttling of fully folded protein cargo across peroxisomal membranes(Lanyon-Hogg et al., 2010; Van Veldhoven and Baes, 2013; Wanders, 2014). Thus, disruptions in PEX proteins could alter biosynthesis and/or degradation of target substrates leading to PBD in humans.

The zinc RING-finger peroxin, PEX10, is necessary for peroxisome assembly, for import of target substrates, and for recycling or degradation of protein complexes and amino acids(Oeljeklaus et al., 2012; Williams et al., 2008; Williams et al., 2012). For example, PEX10 binds to PEX5 and helps dock PEX5 at the pore to allow cargo import. Moreover, PEX10 and the conserved RING domain peroxisomal integral membrane proteins PEX2 and PEX12 act as E3-ubiquitin ligases (Platta et al., 2009; Williams et al., 2012). The RING peroxins serve to mono- or poly-ubiquitinate PEX5 to control PEX5 receptor recycling or degradation. Poly-ubiquitinated PEX5 is sent to the proteasome for degradation whereas mono-ubiquitination of the PEX5 receptor allows it to return to the cytosol where it can bind new protein cargo for import into the peroxisomes (Agne et al., 2003; Chang et al., 1999b; Thoms and Erdmann, 2006).

Mice lacking neural *Pex5* develop postnatal neurological defects with motor dysfunction due to defects in axon integrity, demyelination and neuroinflammatory reactions (Bottelbergs et al., 2012; Hulshagen et al., 2008; Krysko et al., 2007), suggesting a neural basis to the etiology of PBD in patients with mutations in PEX5. Neurological defects such as cerebellar ataxia, spinal ataxia, progressive ataxia and reduced cognitive capacity are diagnoses in patients with mutations in the *PEX10* gene (Steinberg et al., 2004; Warren et al., 2000). However, no published vertebrate model exists with a mutation in *Pex10*. Thus, it is unclear

how the loss of vertebrate PEX10 contributes to PBD disease pathology. Here, we identify a mouse model with a mutation in *Pex10* that causes neonatal mortality and defects in embryonic locomotion. Furthermore, we characterize the biochemical defects and pathology of *Pex10* mutant mice. *Pex10* homozygous mutants display prenatal pathology including defects in axonal integrity, decreased Schwann cell number and defects at the neuromuscular interface. Therefore, this *Pex10* model provides new insight into the embryological origin of PBD pathology and highlights the role of peroxisomes in embryonic peripheral nervous system development.

Material and Methods

Forward Genetic Screen and Identification of the *Pex10* Mutation

ENU mutagenesis was performed as described (Kasarskis et al., 1998) on males of C57BL/6J background and then outcrossed onto 129S1/Svlmj background to score G3 embryos at embryonic day 18.5 for recessive mutations that affect embryonic locomotion. Through meiotic mapping which followed linkage between the non-motile phenotype and C57BL/6J markers, the genetic region containing the mutation that affected locomotion was first mapped to the proximal third of chromosome 4 using a panel of 96 MIT and SKI SSLP markers and then narrowed to a 7Mb region by the use of additional MIT SSLP markers on the telomeric end of chromosome 4. DNA from phenotypic mutant embryos (n=4) was sent to the Broad Institute to identify all C57BL/6J regions, which confirmed localization to a 3Mb interval of the telomeric region of chromosome 4. DNA from phenotypic embryos was sent for whole exome enrichment followed by next generation sequencing (Otogenetics, Inc) and this identified only 1 candidate homozygous variant in the *Pex10* gene within the surrounding 20 Mb region of chromosome 4. This variant was a single base substitution (G to A) that introduces a C294Y non-synonymous amino acid change. Using Ensembl Genome Browser (ensembl.org) combined with whole exome capture data analysis, PEX genes and genes involved in peroxisome function (ABC transporter family and PPAR family) were subsequently examined yet no homozygous variants in exon sequences were found, other than the *Pex10* mutation. To confirm the mutation in *Pex10*, genomic DNA in overlapping segments of the *Pex10* gene was amplified by PCR from phenotypic E18.5 embryos and compared with control E18.5 C57Bl/6J DNA. Subsequently, embryos were genotyped as follows: Tissue was placed in tail lysis buffer (100 mM Tris.Cl pH8.0, 5 mM EDTA, 0.2% SDS, 200 mM NaCl) overnight. DNA was amplified using Taqman Gold (Applied Biosystems) with primer set to *Pex10* (forward primer: AGAACCCTCATCCATTTGCCTGGT; reverse primer: AAAGTACCTCAAGCTCCCTGCACA. PCR amplification was performed for 35 cycles at 55°C. PCR product was sent to Barbara Davis Center Molecular Biology Service Center at the University of Colorado Denver for sequencing. The official nomenclature of this mutant allele is $Pex10^{m1Nisw}$, but for simplicity we will use $Pex10^{CY}$ throughout the manuscript. All of the data presented here were obtained after outcrossing > generations onto 129S1/Svlmj background.

Mouse Embryonic Touch Assay

This touch assay was designed to examine the spinal locomotor response from the activation of the muscle spindles that carry signals to the dorsal root ganglion, to the interneuron relays between the dorsal root ganglion and motoneurons, and the motoneuron activation of the muscle to induce a contraction. Embryos were dissected from timed pregnant dams and placed in room temperature oxygenated mouse Tyrode's solution. To induce limb movement, the foot-pads were pinched with tweezers. For example in E18.5 wildtype embryos, pinching induces paw retraction and cross-extensor reflexes. Both forelimb and hindlimb were assayed and retraction of the limb was scored as 1, no retraction of limb was scored as 0 and slow or modest retraction of limb was scored as 0.5. We also scored for S-shaped movements in axial muscles by touching the forceps to the dorsal rib cage. Touch assay was performed on each litter to identify phenotypic embryos. The genotype of all embryos was confirmed as above.

Biochemical Analysis

Bloodspots were collected from E18.5 embryos and from adult mice (>2 months old) on filter paper (Whatman 903, GE Lifesciences). Markers of PBD were analyzed by the Peroxisomal Diseases Laboratory within the Moser Center for Leukodystrophies at the Kennedy Krieger Institute (Baltimore, MD). Human samples from normal control and individuals with PBD and rhizomelic chondrodysplasia punctacta (RCDP) were collected and analyzed by the Kennedy Krieger Institute and only the data without identifying information was provided. Lyso-phosphatidylcholines, (lyso-PCs), including C26:0 lyso-PC, peroxisomal bile acid intermediates and plasmalogens were analyzed by combined liquid chromatography–tandem mass spectrometric (LC–MS/MS) method (Hubbard et al., 2009; Hubbard et al., 2006; Johnson et al., 2001; Zemski Berry and Murphy, 2004).

Cell Culture

Mouse embryonic fibroblasts (MEFs) were isolated from E18.5 limb dermis. Dermis was removed from limbs and cut into small fragments and dissociated in 0.25% trypsin-EDTA (Gibco) for 15 minutes at 37°C. Fragments were sheared by 5 passes through a 1000 μl pipette in DMEM/F12 (Gibco) with 10% FCS (Gibco). Suspension was centrifuged and re-suspended in DMEM/F12 medium consisting of 10% FCS, penicillin/streptavidin (Gibco) and L-glutamine (Gibco). Cells were re-plated at least once before experimentation.

Peroxisomal Localization

For peroxisomal localization studies, a 'LQSKL' PTS1 signal sequence from acyl-CoA oxidase was appended to the C-terminus of an EGFP reporter construct (in pCDNA3.1) using PCR. MEFs from wild-type or homozygous mutant *Pex10*^{CY} embryos were plated on 18-mm glass coverslips in DMEM/F12 (Gibco) with 10% FBS, and transiently transfected with the EGFP-SKL reporter using MEF 2 Nucleofector Kit (Lonza) according to the manufacturer's protocol. 24 hours after transfection, cells were fixed using 4% paraformaldehyde and imaged on an Olympus IX71 microscope equipped with a spinning disc scan head (Yokogawa Corporation of America) with a 60×/NA 1.4 objective. 488-nm excitation illumination was delivered from an AOTF controlled laser launch (Andor

Technology) and images collected on a 1024 × 1024 pixel EM-CCD camera (iXon; Andor Technology).

Docosahexaenoic Acid Study

Docosahexaenoic Acid (DHA) was obtained from Cayman Chemical Company (Michigan, USA). After detection of a vaginal plug, *Pex10* heterozygous females received drinking water supplemented with 50 μM of DHA, throughout the entire gestation. The DHA concentration used was determined according to Correia et al (Correia et al., 2012), which showed gestational affects of DHA on gastric mucosa colonization.

Electron Microscopy

Sciatic nerves from E18.5 embryos were dissected and fixed with 2% paraformaldehyde/ 2.0% glutaraldehyde in phosphate buffer (pH 7.2) for 1 hour at room temperature. Nerves were transferred to 2.0% glutaraldehyde in 0.1 M phosphate buffer (pH 7.2) overnight at 4°C. The sciatic nerve was dissected into segments, followed by a secondary post-fixation in 2% osmium tetroxide and 1.5% potassium ferrocyanide in phosphate buffer for 1 hour at room temperature. Samples were dehydrated through sequential ethanol rinses (50, 70, 90, 95 and 100% ETOH) and embedded in Epon/Araldite resin and polymerized overnight at 60°C. Ultrathin sections were cut, placed on copper mesh grids and double contrasted with 2% aqueous uranyl acetate and Reynold's lead citrate. Due to artifacts present at the peripheral regions of the cross sections, only the central region of the sciatic nerve was examined. Grids were photographed using a FEI Technai G2 BioTwin transmission electron microscope.

Immunohistochemistry

Wildtype and mutant MEFs were fixed in 4% paraformaldehyde for 10 minutes then permeabilized with 0.1% Triton/PBS for 30 minutes. Non-specific binding was blocked with 2% fetal bovine albumin (Sigma) for 30 minutes. Primary antibody to catalase at 1:500 (Sigma) was added for 1 hour at room temperature. Secondary antibody (Alexa Fluor 488, 1:800, Molecular Probes) was applied for 1 hr before washing and mounting.

Embryos were dissected and pinned to a Sylgard-coated dish in 4% paraformaldehyde for 1 hour. Embryos were placed in 5% sucrose for 1 hour at room temperature before transfer into 30% sucrose overnight at 4°C followed by embedding in OCT. Frozen sections at 10 μm thickness through the spinal column were collected and fixed in 1% paraformaldehyde for 10 minutes. Conditions for immunolabeling are described below. TUNEL labeling was according to manufactures instructions (Millipore). After TUNEL labeling, Hoechst 33342 (Life Technologies) was added for 15 minutes at room temperature.

Muscles were dissected and pinned to a Sylgard-coated dish in 4% paraformaldehyde for 10 min then permeabilized with 0.2% Triton/PBS for 30 minutes. α-BTX conjugated Alexa 555 and Alexa 647 (1:500, Life Technologies) were used for labeling of acetylcholine receptors (AChRs) at the membrane. Non-specific reactivity was blocked with 2% BSA/PBS for 1 hour. Primary antibodies for β-tubulin III (1:1000, Covance), S100B (1:1000, Sigma; S2644 used for E18.5 sciatic; HPA015768 used for E15.5 sciatic) neurofilament-M (1:100; Sigma)

and synaptophysin (SV2, 1:200; DSHB) were applied overnight at 4°C. Secondary antibodies (Alexa Fluor 488 and Alexa Fluor 568-conjugated to specific primary, 1:800, Molecular Probes) were applied for 1 hr.

Confocal microscopy

Immunolabeled samples were examined on a Zeiss LSM 510 confocal laser scanning microscope. Emitted fluorescence was directed to a photomultiplier with long-pass filter. Confocal fluorescence intensity data were recorded as the average of four line scans per pixel and digitized at 8-bits, with photomultiplier gain adjusted such that maximum pixel intensities were <70% saturated.

Sharp Electrode Recordings

Current-clamp sharp electrode recordings were performed as described (Plomp et al., 1992). E18.5 diaphragms were dissected and kept at room temperature in mouse Normal Ringers. Diaphragm muscle fibers were impaled with glass capillary microelectrode (30 MΩ resistance) made using a P-97 microelectrode puller (Sutter Instruments) and filled with 3 M KCl (Brown et al., 2008). Evoked responses were elicited by a 0.2-ms maximal stimulus applied to the phrenic nerve using a suction electrode and pulse generator (STG 1002, ALA Scientific Instruments). Evoked and miniature endplate potentials (MEPP) were recorded using an Axoclamp-2A amplifier (Axon Instruments) and DigiData 1322A (Molecular Devices). Muscle fiber membrane potentials were adjusted to E_m= −70 mV under current clamp. Data was extracted and analyzed with Axoscope 10 software (Molecular Devices).

Quantification

In wildtype spinal cord cross sections, white matter is clearly delineated by rostral and caudal axon tracks and revealed using antibodies to Medium Neurofilament (NF-M: NF-160) and β-tubulin III (β-TubIII). The white matter tracks were captured as a region of interest (ROI) by Zen 2009 software (Ziess). The intensities of β-TubIII and NF-M were quantified within the ROI. A ratio of NF-M intensity to the β-TubIII intensity was produced for each white matter region. This data was normalized to control white matter NF-M: β-TubIII intensity. The level of β-TubIII brightness was equally decreased in Figures 2G–K to visualize NF-M labeling.

The soleus muscle and ventral quadrant of the diaphragm are easily identified by the stereotypical pattern of innervation and AChR cluster placement. These muscles in wildtype embryos show a high degree of reproducibility in axon branching, endplate number and distribution. In diaphragms, endplate region was quantified by drawing a line between the most distal α-BTX positive endplates every 0.2 mm on each side of the centralized phrenic nerve in the ventral diaphragm quadrant in comparison to the total width of the diaphragm. Percentage of AChR clusters was performed on compressed zstack images. Endplate number was quantified on z-stack images of entire muscle by dividing the ventral quadrant into 0.1 mm bins from central branch in ventral quadrant. The Zen 2009 software then calculated the size of the endplates.

Statistical Analysis

The unpaired two-tailed Student's t test was used to compare means for statistical differences. Unless otherwise mentioned n>5 for all experiments. Data in the manuscript are represented as mean ± SEM unless otherwise indicated. $P < 0.05$ was considered significant.

Study Approval

All experiments were conducted in accordance with the protocols described in the Guide for the Care and Use of Laboratory Animals (NIH. Revised 2011).

Results

Forward Genetic Screen for Locomotor Defects Identifies a Mutation in *Pex10*

Through a chemically induced mutagenesis screen in mice, we identified a recessive mutation in which homozygous mutant embryos display a progressive loss of limb movement from embryonic day 17.5 (E17.5) to birth (Figure 1A). At birth, these mice show an inability to breath, turn blue, and die shortly thereafter (Figure 1B). Meiotic mapping, whole exome enrichment, and next generation sequencing (NGS) identified a homozygous point mutation in the peroxisomal biogenesis factor 10 (*Pex10*) gene on chromosome 4 in embryos with locomotor deficits (184/184 reads). This single G to A nucleotide change creates a C294Y non-synonymous amino acid change (Figure 1C) that would be expected to disrupt the crucial second zinc RING finger binding domain (C_3HC_4) important for E3 ligase activity in PEX10. This corresponds to amino acid 316 in human PEX10. The mutant line is called $Pex10^{m1Nisw}$ and for simplicity we refer to it here as $Pex10^{CY}$. No other peroxisomal factor showed a homozygous or heterozygous variant by whole exome enrichment and NGS. While mutations at amino acid 316 in humans have yet to be discovered, mutations at 310 and 314 are associated with NALD and Zellweger syndrome(Krause et al., 2006; Warren et al., 1998). The great majority of $Pex10^{CY/CY}$ mice die within the first few hours of birth although two survived (<2%; 2 of 132 confirmed homozygous mutations). These survivors showed a severe decrease in size and weight (Figure 1D, E) and an ataxic gait. Ataxia is also observed in humans with *PEX10* mutations.

Testing for peroxisomal biogenesis disorders often involves harvesting and examination of human fibroblasts for peroxisomal markers such as the enzyme catalase. Patients with *PEX10* mutations have cytosolic catalase staining but lack catalase staining in peroxisomes (Chang et al., 1999a; Chang et al., 1999b). In fibroblasts from wildtype mice, catalase staining shows a punctuate pattern of immunofluorescence typical of peroxisomes (Figure 1F). In contrast, fibroblasts derived from E18.5 $Pex10^{CY/CY}$ embryos show only diffuse staining in the cytoplasm (Figure 1G). To examine peroxisomal targeting, EGFP fused to a PTS1 peroxisomal targeting signal 'SKL' (EGFP-SKL) was transfected into fibroblasts. In wildtype fibroblasts, EGFP-SKL was expressed in a punctuate expression pattern typical of peroxisomes (Figure 1H). However, in fibroblasts derived from $Pex10^{CY/CY}$ embryos, EGFP-SKL was expressed in a diffuse pattern, suggesting that $Pex10^{CY/CY}$ fibroblasts lack peroxisomal import of EGFP-SKL (Figure 1I). These results indicate the PTS1 peroxisomal targeting signal pathway for import of peroxisomal matrix proteins is disrupted in the mutant

fibroblasts. Taken together, our genetic screen identified a mouse *Pex10* model that can be used to study the embryological basis of PBD neurological deficits.

Biochemical Abnormalities in *Pex10*$^{CY/CY}$ Mice

Despite the evidence that PBD phenotypes can be observed at birth in human patients (Steinberg et al., 2006; Wanders and Waterham, 2005, 2006) and in our mouse model, it appears that biomarkers of peroxisomal function have not been examined during late embryonic development. Thus, we evaluated PBD markers at E18.5, when the locomotor defect was apparent. Blood samples were collected from E18.5 embryos, adult control mice, the heterozygous (*Pex10*$^{CY/+}$) birthing females and the two *Pex10*$^{CY/CY}$ adults to assay for erythrocyte plasmalogens, VLCFA, and bile intermediates for comparison to patient samples of PBD and ZS. In the *Pex10*$^{CY/CY}$ embryos, plasma VLCFA levels were ~10-fold higher (C26:0-LPC%; n=8) compared to wildtype littermates (n=10; Table 1). Conversely, total plasmalogen levels were ~21-fold lower in *Pex10*$^{CY/CY}$ embryos relative to wildtype littermates (Table 1). Thus, VLCFA was elevated and plasmalogen levels decreased in *Pex10*$^{CY/CY}$ embryos, in a similar trend as that seen in human PBD patients. Subtle variations in plasmalogens were detected in *Pex10*$^{CY/CY}$ adult mice that survived birth, which is intriguing but we could not determine significance as only two animals survived over the course of these studies. Peroxisomal bile acid intermediates as measured by 3,7-dihydroxy-5-colest-26-oic acid (DHCA) and 3,7,12-trihydroxy-5-cholestan-26-oic acid (THCA) were ~11 fold and ~28 fold increased in *Pex10*$^{CY/CY}$ embryos compared to wildtype littermates (Table 1); however, the levels were not in the range found in patients with PBD or rhizomelic chondrodysplasia punctata (RCDP), which is a non-leathal disease due to a mutation in PEX7(Table 1). This difference may be due to differences between mouse and human, between fetal and postnatal development, or the *Pex10* mutation. Nevertheless, our data provide evidence that peroxisomal function and spinal locomotor function are severely disrupted in *Pex10*$^{CY/CY}$ mutant embryos, and that the *Pex10* mutant model reflects a number of peroxisomal biochemical hallmarks identified in human PBD patients.

PEX10 is a major component of the peroxisome needed for both biosynthesis and degradation of proteins and fatty acids. We attempted to decrease the embryonic mortality by providing a diet of docosahexaenoic acid (DHA) to pregnant dams from vaginal plug to birth. However, homozygous neonates were cyanotic and died shortly after birth at a normal Mendelian ratio (17:36:15). At weaning ages, we did not observe an increase in *Pex10*$^{CY/CY}$ survivors.

Spinal cords of *Pex10*$^{CY/CY}$ embryos show no apoptosis defect

Plasmalogens, which are synthesized in peroxisomes and which are deficient in PBDs, are critical for neural (neurons and glial) cell survival and plasmalogens are a significant component of the glial myelin sheath. To determine whether locomotion defects were a consequence of apoptosis of neurons and glia that control limb movement, we performed TUNEL labeling. We examined E18.5 cervical and lumbar enlargements where the fore- and hindlimb motoneurons are located from *Pex10*$^{CY/CY}$ embryos with immobile hindlimbs but mobile forelimbs compared to wildtype littermates. No significant differences were

detected in the number of apoptotic cells at cervical or lumbar levels or in the sensory neurons within the dorsal root ganglion (DRG) (Figure 2A–F; actual cell counts presented in legend to Figure 2) This data suggests that apoptosis does not underscore the locomotive defects in *Pex10*$^{CY/CY}$ embryos.

The hallmark of severe peroxisomal biogenesis disorders is demyelinated white matter tracks in the central nervous system. Decreased peroxisomal function in oligodendrocytes leads to the accumulation of VLCFA which is damaging for the nervous system(Baes and Aubourg, 2009; Kassmann et al., 2007). VLCFA induce oxidative stress and decreased peroxisomal fuction in oligodendrocytes (Baarine et al., 2012). Therefore, we examined the axons in the white matter regions at lumbar and cervical enlargement levels of the spinal cord of E18.5 *Pex10*$^{CY/CY}$ embryos and littermate controls. Medium Neurofilament (NF-M) labeling was utilized to identify fiber track defects in axon integrity, while β-tubulin III labeling was utilized for baseline labeling of all neurons. Spinal cord cross sections at the level of the cervical enlargement showed no significant difference between *Pex10*$^{CY/CY}$ and littermate controls (Figure 2G–I; intensity of NF-M/β-tubulin III normalized to control was 0.92+/−0.08 in *Pex10*$^{CY/CY}$, 3 embryos; $p>0.05$). However, at the lumbar level, *Pex10*$^{CY/CY}$ embryos that were hindlimb immobile showed a significant decrease in NF-M labeling compared to littermate controls (Figure 2J–L, 0.31+/−0.12 in *Pex10*$^{CY/CY}$, 3 embryos; $p=0.004$). This data points to defects in axon integrity in white matter tracks of *Pex10*$^{CY/CY}$ embryos and this may in part underscore the hindlimb immobility defect.

Progressive Developmental Defect in *Pex10*$^{CY/CY}$ Axon Integrity

Motoneuron axons enter white matter tracks within the spinal cord prior to exit into the periphery to innervate muscle in a stereotypical pattern (Hanson and Landmesser, 2003). Demyelination and degeneration of the central nervous system in patients with PBD has been the focus of previous studies. In an animal model of *Pex7* mutation leading to non-lethal RCDP, defects in myelination and remyelination within the peripheral nervous system were detected in postnatal and adult animals (da Silva et al., 2014). Here we asked whether a PNS abnormality might have an embryological origin, which could lead to progressive embryonic locomotor defects. Schwann cells are the principal glia cells that myelinate the PNS. At E18.5, Schwann cells encapsulate multiple motor axons (Jessen and Mirsky, 2005) and muscle innervation by the sciatic nerve is completed. Utilizing electron microscopy (EM) at E18.5, cross sections of dissected sciatic nerves from hindlimbs of wildtype embryos showed Schwann cells encapsulating axon bundles within the central region of the sciatic (Figure 3A). In contrast, *Pex10*$^{CY/CY}$ sciatic axons lacked conventional bundling, there was no evidence of Schwann cells with normal morphology near axons and, instead, flattened fibroblast-like cells were present (Figure 3B). This data suggests defective axon bundling by Schwann cells and axonal defects in embryonic *Pex10*$^{CY/CY}$ sciatic nerves.

To explore further the defect in axon-Schwann cell interaction in *Pex10*$^{CY/CY}$ sciatic nerves, cross sections of E18.5 sciatic nerves were labeled with antibodies to NF-M to label axons, S100B to label Schwann cells and Hoechst to label nuclei. Littermate control sciatic nerve cross sections showed S100B positive Schwann cells, and NF-M positive axons throughout the section (Figure 3C–F). In contrast, cross sections of *Pex10*$^{CY/CY}$ sciatic nerves showed

S100B and NF-M positive cells around the perimeter but these markers were greatly reduced in intensity within the central regions of the nerve, although nuclei were present (Figure 3G–J). The E18.5 antibody labeling and EM data suggest defects in axonal integrity, perhaps due to defective Schwann cell function. We then examined axon and Schwann cell labeling of the sciatic nerves at an earlier time point, E15.5. This showed that E15.5 wildtype and *Pex10*$^{CY/CY}$ embryos had similar levels of NF-M and S100B reactivity (Fig. 3K–R). The normal labeling at E15.5 but disrupted labeling at E18.5, combined with the EM data, is consistent with the normal movement of *Pex10*$^{CY/CY}$ embryos at early fetal stages but progressive loss of movement at later fetal stages. Together these data suggest that the progressive loss of hindlimb movement corresponds to a progressive developmental defect in axon integrity of *Pex10*$^{CY/CY}$ sciatic nerves.

Synaptic machinery defects in *Pex10*$^{CY/CY}$ hindlimb muscle

The defects in axon integrity in *Pex10*$^{CY/CY}$ sciatic nerves might suggest deterioration of neuromuscular synapses in hindlimb muscles. Axons extend within muscles to form neuromuscular synapses or junctions (NMJ). Acetylcholine (ACh) is transmitted by action potential induced vesicular release onto ACh receptors (AChR) in the juxtaposed muscle fiber. This pre-synaptic ACh release induces a global change in muscle calcium levels leading to muscle contractions. To examine the structure of the NMJ, antibodies were used to label the axon (neurofilament NF-M), pre-synaptic vesicles (SV2) and post-synaptic AChR clusters (α-bungarotoxin, α-BTX). Soleus muscles from E18.5 littermate controls showed co-localization of axons, synaptic vesicles and AChR clusters (Fig. 4A–D). *Pex10*$^{CY/CY}$ soleus muscle showed decreased co-localization of axons with AChR clusters (Fig. 4E–H). Moreover, several axons with adjacent AChR clusters lacked synaptic vesicle labeling (quantification of results in Fig. 4 I, J). This data suggests structural deficits in *Pex10*$^{CY/CY}$ hindlimb synapses. Together, the identified defects in synaptic machinery of the hindlimb muscle and in axon integrity of the sciatic nerve may point to an embryonic neurodegenerative-like disorder underlining the progressive loss of movement in *Pex10*$^{CY/CY}$ embryos.

Defects of axons, Schwann cells and synapses in *Pex10*$^{CY/CY}$ diaphragm muscles

In patients with neurodegenerative disorders, such as amyotrophic lateral sclerosis (ALS), immobility is progressive, first affecting the legs, followed by arms and finally the axial musculature, which affects respiration. The lack of respiration in *Pex10*$^{CY/CY}$ mutant mice at birth led us to examine innervation of the diaphragm muscle during two stages of fetal development. At E15.5, *Pex10*$^{CY/CY}$ and littermate control diaphragms showed similar AChR cluster patterning (Figure 5A–C; α-BTX). However, many phrenic axons in E15.5 *Pex10*$^{CY/CY}$ mutant embryos extended abnormally beyond the AChR clusters (Figure 5A–C, F; axons labeled by NF-M and SV2). E18.5 *Pex10*$^{CY/CY}$ embryos with modest forelimb movement showed highly significant extension of the axons beyond the relatively normally distributed AChR clusters, although within the central region of the diaphragm the axons were directly juxtaposed to the AChR clusters (Figure 5E, F). This data suggests that *Pex10*$^{CY/CY}$ axons do not halt axon extension after synapse formation.

The mechanisms involved in halting axon extension in muscle during synaptogenesis are not well understood, but likely require signals intrinsic to the developing axons as well as extrinsic signals derived from Schwann cells and the target muscle. During peripheral nerve regeneration, Schwann cells are crucial in aiding the navigation of axons to synaptic sites in muscle (Kang et al., 2003; Son and Thompson, 1995). During embryonic development, immature Schwann cells and terminal Schwann cells might have a similar role in the early formation and maintenance of the NMJ. The reduced labeling with the Schwann cell marker and aberrant Schwann cell morphology by EM of E18.5 *Pex10*$^{CY/CY}$ sciatic nerve led us to evaluate Schwann cells in the diaphragm muscle using an antibody to SOX10 which localizes to Schwann cell nuclei along axons and at synapses (Figure 5G, H: green label). E18.5 *Pex10*$^{CY/CY}$ diaphragm had a significant decrease in SOX10 positive cells located terminally on axons (Figure 5 G–I; control: 89.9 +/− 6.8% of nerves with a SOX10 positive terminal cell; n=4 compared to *Pex10*$^{CY/CY}$: 35 .3+/−6.1; n=4) and adjacent to axons (Figure 5J; control: 0.062+/−0.012 SOX10 positive nuclei/μm of nerve; n=4 compared to *Pex10*$^{CY/CY}$: 0.026+/−0.011μm; n=4). The percent of SOX10 positive cells juxtaposed to AChR clusters was also reduced compared to littermate control embryos (Figure 5G–K; control: 92.4+/−3.2; n=4 compared to *Pex10*$^{CY/CY}$: 56.9+/−8.8; n=4). These data suggest that *Pex10*$^{CY/CY}$ diaphragms have defects in proper Schwann cell placement at neuromuscular junctions.

Together, the differences observed between *Pex10*$^{CY/CY}$ and control diaphragms in the phrenic nerve, Schwann cells and synapses may result in altered synaptic transmission at the neuromuscular junction. The NMJ releases small packets of neurotransmitter spontaneously, termed spontaneous release, or action potential transmitter release, termed evoked release. Spontaneous neuromuscular synaptic activity, as measured by miniature endplate potential (MEPP) frequency (events per minute) in muscle, was unchanged in E18.5 *Pex10*$^{CY/CY}$ diaphragm (0.85 ± 0.25, n = 18 cells, n = 3 embryos, 70 total events in 82 min) compared with wildtype diaphragm (0.72 ± 0.31, n = 16 cells, n = 3 embryos, 67 total events in 93 min; p>0.05; Fig.6A–C). Examinations of the amplitudes of MEPP showed no variability between *Pex10*$^{CY/CY}$ muscles (1.99 ± 0.15 mV, n = 18 cells and 3 embryos) compared with wildtype (2.01 ± 0.14 mV, n = 16 cells and 3 embryos; p>0.05; Fig. 6A, B, D).

To examine motor axon functional physiology, action potential evoked endplate potentials (EPP) were induced by stimulation of the phrenic nerve. EPP amplitudes were significantly decreased in *Pex10*$^{CY/CY}$ muscles (17.29 ± 3.29 mV, n = 16 cells and 3 embryos) compared to control (30.17 ± 7.16 mV, n = 14 cells and 3 embryos; Fig. 6E–G). EPP stimulation induced muscle contractions in control and *Pex10*$^{CY/CY}$ muscles (arrow in Figure 6E, G). These data suggest that synaptic transmission at the diaphragm is present, although diminished, in E18.5 *Pex10*$^{CY/CY}$ diaphragms.

Discussion

Zellweger syndrome, NALD, cerebellar ataxia, spinal ataxia, and progressive ataxia are diagnoses in patients with mutations in *PEX10* (Steinberg et al., 2004; Warren et al., 2000). Despite the fact that neurological deficits can be observed at birth in some PBD patients including those with *PEX10* mutations, the embryological basis of the disease is unclear.

Here, we present a mouse model of PBD that illuminates defects in the spinal locomotion circuit prior to birth. First, we identified a mutation in *Pex10* that causes neonatal mortality and progressive loss of movement during embryogenesis, prior to the onset of cerebellar inputs that do not develop until after birth. Second, $Pex10^{CY/CY}$ embryos acquire pathological and biochemical hallmarks similar to patients with PBD. Third, white matter, sciatic nerves, and motor axons innervating hindlimb muscles in $Pex10^{CY/CY}$ embryos display characteristic signs of defects in axon integrity. Fourth, Schwann Cells are decreased in number and misplaced along axons and synapses of muscles in $Pex10^{CY/CY}$ embryos. Fifth, phrenic nerves of $Pex10^{CY/CY}$ embryos extend their axons beyond AChR clusters, and display decreased action potential release of transmitter onto the muscle.

During embryogenesis, nutrients are provided across the placenta to the embryos. However, poly-unsaturated fatty acids, such as plasmalogens, are locally synthesized by the embryo (Janssen et al., 2000). Our biochemical analyses of $Pex10^{CY/CY}$ embryos show that PEX10 is required for embryonic plasmalogen synthesis in mice. The finding of aberrant biomarkers in the mutant mouse embryos suggests the possibility of prenatal screening for peroxisomal dysfunction. *Pex2* and *Pex5* deficient neonates also show decreased synthesis of plasmalogens and increased plasma VLCFA (Baes et al., 1997; Faust and Hatten, 1997) and PEX2 and PEX5 function with PEX10 for cargo import and plasmalogen synthesis (Oeljeklaus et al., 2012; Williams et al., 2008; Williams et al., 2012). Both *Pex2* and *Pex5* deficient mice die shortly after birth from what was considered a feeding defect and not a respiratory defect (Baes et al., 1997; Faust and Hatten, 1997). On a congenic 129svJ background, the same background examined in our study, *Pex2* deficient mice showed a 20% increase in embryonic mortality (Faust and Hatten, 1997). Tissue-specific knock-out of *Pex5* in the liver allowed survival but resulted in persistent cerebellar atrophy, whereas conditional knock-out of *Pex5* in neurons and Schwann cells also allowed survival but resulted in cortical migration and demyelination abnormalities as well as increased neuroinflammatory response (Bottelbergs et al., 2012; Hulshagen et al., 2008; Krysko et al., 2007). The differences in mortality of $Pex10^{CY/CY}$ mutants and other PEX deficient mouse models might be due to differences in genetic background, the genetic allele, or partial compensation of function. In the future it will be of interest to determine whether decreased axon integrity is a common feature of peroxisomal dysfunction. In patients with PBD, mutations in PEX genes are likely to induce protein dysfunction and less likely to eliminate protein expression (Steinberg et al., 2006; Wanders and Waterham, 2005, 2006). Future studies in animal models exploiting the use of mixed and congenic backgrounds, conditional knock-outs, and hypomorphic alleles will help to elucidate the role of peroxisomal biogenesis factors in embryonic and neonatal neurodevelopment.

The *Pex10* mutant identified here provides a model to evaluate PNS pathology that leads to progressive locomotor defects. Schwann cells are the principle myelinating glia cells of the PNS. Schwann cells target and wrap the motor axon while the terminal Schwann cells encapsulate the NMJ for proper locomotion (Pincon-Raymond et al., 1987). PEX7 has been implicated in Schwann cell myelination and remyelination and plasmalogen synthesis in postnatal and adult mice (da Silva et al., 2014). PEX7 requires E3 ligase activity of PEX10 for cargo import (Titorenko and Rachubinski, 2001a, b). Our data demonstrate defects in

Schwann cell form and function during embryogenesis and prior to axonal myelination (Martin and Webster, 1973; Webster et al., 1973). Early during murine embryogenesis (E14.5–15.5), Schwann cells encapsulate bundles of motor axons and form a terminal cap at the synapse, which helps stabilize the synapse (Jessen and Mirsky, 2005; Reddy et al., 2003). The early events that lead to the formation and stability of the NMJ at embryonic stages are essential for the function of the NMJ in adult muscle. The respiratory defects of the *Pex10*$^{CY/CY}$ mice at birth and aberrant Schwann cell numbers suggest that communication between the spinal cord and diaphragm is impaired. Moreover, the abnormal sprouting of the phrenic nerve and decreased EPP amplitude in the E18.5 diaphragm suggests failure to establish or maintain stable synaptic connections. Our model suggests that progressive motor loss in *Pex10*$^{CY/CY}$ mice might be due to failure to stabilize the synapse during fetal development, at least in part due to abnormal Schwann cell function, followed by progressive loss of axon integrity.

In summary, the *Pex10* mutant mouse presents a novel and valuable model for examination of embryonic deficits due to PBD. Our data illustrates the importance of PEX10 during the early formation of the spinal locomotion circuit, axonal integrity and synapse formation. PBDs due to *Pex* mutations affect peroxisome function (Braverman et al., 2013; Steinberg et al., 2006), similar to what is observed in the *Pex10*$^{CY/CY}$ model. Therefore, the pathology described in the PNS of *Pex10*$^{CY/CY}$ mice may be common for all PBD that display hypotonia and defects in locomotion at birth.

Acknowledgments

We thank Lori Bulwith for technical assistance and Rosa Moreno at the University of Colorado for comments on the manuscript. We would like to thank Ann Moser at the Kennedy Krieger Institute for providing the data in Table 1. This work was supported by postdoctoral fellowships from MDA69338 and NIH F32 NS059267 (MGH) and by NIH R21 NS085749. LN is an investigator of the Howard Hughes Medical Institute.

References

Agne B, Meindl NM, Niederhoff K, Einwachter H, Rehling P, Sickmann A, Meyer HE, Girzalsky W, Kunau WH. Pex8p: an intraperoxisomal organizer of the peroxisomal import machinery. Mol Cell. 2003; 11:635–646. [PubMed: 12667447]

Baarine M, Andreoletti P, Athias A, Nury T, Zarrouk A, Ragot K, Vejux A, Riedinger JM, Kattan Z, Bessede G, Trompier D, Savary S, Cherkaoui-Malki M, Lizard G. Evidence of oxidative stress in very long chain fatty acid--treated oligodendrocytes and potentialization of ROS production using RNA interferencedirected knockdown of ABCD1 and ACOX1 peroxisomal proteins. Neuroscience. 2012; 213:1–18. [PubMed: 22521832]

Baes M, Aubourg P. Peroxisomes, myelination, and axonal integrity in the CNS. Neuroscientist. 2009; 15:367–379. [PubMed: 19666893]

Baes M, Gressens P, Baumgart E, Carmeliet P, Casteels M, Fransen M, Evrard P, Fahimi D, Declercq PE, Collen D, van Veldhoven PP, Mannaerts GP. A mouse model for Zellweger syndrome. Nat Genet. 1997; 17:49–57. [PubMed: 9288097]

Bottelbergs A, Verheijden S, Van Veldhoven PP, Just W, Devos R, Baes M. Peroxisome deficiency but not the defect in ether lipid synthesis causes activation of the innate immune system and axonal loss in the central nervous system. J Neuroinflammation. 2012; 9:61. [PubMed: 22458306]

Braverman NE, D'Agostino MD, Maclean GE. Peroxisome biogenesis disorders: Biological, clinical and pathophysiological perspectives. Dev Disabil Res Rev. 2013; 17:187–196. [PubMed: 23798008]

Brown AL, Johnson BE, Goodman MB. Making patch-pipettes and sharp electrodes with a programmable puller. J Vis Exp. 2008

Chang CC, South S, Warren D, Jones J, Moser AB, Moser HW, Gould SJ. Metabolic control of peroxisome abundance. J Cell Sci. 1999a; 112(Pt 10):1579–1590. [PubMed: 10212151]

Chang CC, Warren DS, Sacksteder KA, Gould SJ. PEX12 interacts with PEX5 and PEX10 and acts downstream of receptor docking in peroxisomal matrix protein import. J Cell Biol. 1999b; 147:761–774. [PubMed: 10562279]

Correia M, Michel V, Matos AA, Carvalho P, Oliveira MJ, Ferreira RM, Dillies MA, Huerre M, Seruca R, Figueiredo C, Machado JC, Touati E. Docosahexaenoic acid inhibits Helicobacter pylori growth in vitro and mice gastric mucosa colonization. PLoS One. 2012; 7:e35072. [PubMed: 22529974]

da Silva TF, Eira J, Lopes AT, Malheiro AR, Sousa V, Luoma A, Avila RL, Wanders RJ, Just WW, Kirschner DA, Sousa MM, Brites P. Peripheral nervous system plasmalogens regulate Schwann cell differentiation and myelination. J Clin Invest. 2014; 124:2560–2570. [PubMed: 24762439]

Faust PL, Hatten ME. Targeted deletion of the PEX2 peroxisome assembly gene in mice provides a model for Zellweger syndrome, a human neuronal migration disorder. J Cell Biol. 1997; 139:1293–1305. [PubMed: 9382874]

Hanson MG, Landmesser LT. Characterization of the circuits that generate spontaneous episodes of activity in the early embryonic mouse spinal cord. J Neurosci. 2003; 23:587–600. [PubMed: 12533619]

Hubbard WC, Moser AB, Liu AC, Jones RO, Steinberg SJ, Lorey F, Panny SR, Vogt RF Jr, Macaya D, Turgeon CT, Tortorelli S, Raymond GV. Newborn screening for X-linked adrenoleukodystrophy (X-ALD): validation of a combined liquid chromatography-tandem mass spectrometric (LC-MS/MS) method. Mol Genet Metab. 2009; 97:212–220. [PubMed: 19423374]

Hubbard WC, Moser AB, Tortorelli S, Liu A, Jones D, Moser H. Combined liquid chromatography-tandem mass spectrometry as an analytical method for high throughput screening for X-linked adrenoleukodystrophy and other peroxisomal disorders: preliminary findings. Mol Genet Metab. 2006; 89:185–187. [PubMed: 16828324]

Hulshagen L, Krysko O, Bottelbergs A, Huyghe S, Klein R, Van Veldhoven PP, De Deyn PP, D'Hooge R, Hartmann D, Baes M. Absence of functional peroxisomes from mouse CNS causes dysmyelination and axon degeneration. J Neurosci. 2008; 28:4015–4027. [PubMed: 18400901]

Janssen A, Baes M, Gressens P, Mannaerts GP, Declercq P, Van Veldhoven PP. Docosahexaenoic acid deficit is not a major pathogenic factor in peroxisome-deficient mice. Lab Invest. 2000; 80:31–35. [PubMed: 10653000]

Jessen KR, Mirsky R. The origin and development of glial cells in peripheral nerves. Nat Rev Neurosci. 2005; 6:671–682. [PubMed: 16136171]

Johnson DW, ten Brink HJ, Schuit RC, Jakobs C. Rapid and quantitative analysis of unconjugated C(27) bile acids in plasma and blood samples by tandem mass spectrometry. J Lipid Res. 2001; 42:9–16. [PubMed: 11160360]

Kang H, Tian L, Thompson W. Terminal Schwann cells guide the reinnervation of muscle after nerve injury. J Neurocytol. 2003; 32:975–985. [PubMed: 15034280]

Kasarskis A, Manova K, Anderson KV. A phenotype-based screen for embryonic lethal mutations in the mouse. Proc Natl Acad Sci U S A. 1998; 95:7485–7490. [PubMed: 9636176]

Kassmann CM, Lappe-Siefke C, Baes M, Brugger B, Mildner A, Werner HB, Natt O, Michaelis T, Prinz M, Frahm J, Nave KA. Axonal loss and neuroinflammation caused by peroxisome-deficient oligodendrocytes. Nat Genet. 2007; 39:969–976. [PubMed: 17643102]

Krause C, Rosewich H, Thanos M, Gartner J. Identification of novel mutations in PEX2, PEX6, PEX10, PEX12, and PEX13 in Zellweger spectrum patients. Hum Mutat. 2006; 27:1157. [PubMed: 17041890]

Krysko O, Hulshagen L, Janssen A, Schutz G, Klein R, De Bruycker M, Espeel M, Gressens P, Baes M. Neocortical and cerebellar developmental abnormalities in conditions of selective elimination of peroxisomes from brain or from liver. J Neurosci Res. 2007; 85:58–72. [PubMed: 17075904]

Lanyon-Hogg T, Warriner SL, Baker A. Getting a camel through the eye of a needle: the import of folded proteins by peroxisomes. Biol Cell. 2010; 102:245–263. [PubMed: 20146669]

Martin JR, Webster HD. Mitotic Schwann cells in developing nerve: their changes in shape, fine structure, and axon relationships. Dev Biol. 1973; 32:417–431. [PubMed: 4789699]

Oeljeklaus S, Reinartz BS, Wolf J, Wiese S, Tonillo J, Podwojski K, Kuhlmann K, Stephan C, Meyer HE, Schliebs W, Brocard C, Erdmann R, Warscheid B. Identification of core components and transient interactors of the peroxisomal importomer by dual-track stable isotope labeling with amino acids in cell culture analysis. J Proteome Res. 2012; 11:2567–2580. [PubMed: 22375831]

Pincon-Raymond M, Murawsky M, Mege RM, Rieger F. Abnormal enwrapment of intramuscular axons by distal Schwann cells with defective basal lamina in the muscular dysgenic mouse embryo. Dev Biol. 1987; 124:259–268. [PubMed: 3666308]

Platta HW, El Magraoui F, Baumer BE, Schlee D, Girzalsky W, Erdmann R. Pex2 and pex12 function as protein-ubiquitin ligases in peroxisomal protein import. Mol Cell Biol. 2009; 29:5505–5516. [PubMed: 19687296]

Plomp JJ, van Kempen GT, Molenaar PC. Adaptation of quantal content to decreased postsynaptic sensitivity at single endplates in alpha-bungarotoxin-treated rats. J Physiol. 1992; 458:487–499. [PubMed: 1302275]

Reddy LV, Koirala S, Sugiura Y, Herrera AA, Ko CP. Glial cells maintain synaptic structure and function and promote development of the neuromuscular junction in vivo. Neuron. 2003; 40:563–580. [PubMed: 14642280]

Son YJ, Thompson WJ. Nerve sprouting in muscle is induced and guided by processes extended by Schwann cells. Neuron. 1995; 14:133–141. [PubMed: 7826631]

Steinberg S, Chen L, Wei L, Moser A, Moser H, Cutting G, Braverman N. The PEX Gene Screen: molecular diagnosis of peroxisome biogenesis disorders in the Zellweger syndrome spectrum. Mol Genet Metab. 2004; 83:252–263. [PubMed: 15542397]

Steinberg SJ, Dodt G, Raymond GV, Braverman NE, Moser AB, Moser HW. Peroxisome biogenesis disorders. Biochim Biophys Acta. 2006; 1763:1733–1748. [PubMed: 17055079]

Thoms S, Erdmann R. Peroxisomal matrix protein receptor ubiquitination and recycling. Biochim Biophys Acta. 2006; 1763:1620–1628. [PubMed: 17028012]

Titorenko VI, Rachubinski RA. Dynamics of peroxisome assembly and function. Trends Cell Biol. 2001a; 11:22–29. [PubMed: 11146295]

Titorenko VI, Rachubinski RA. The life cycle of the peroxisome. Nat Rev Mol Cell Biol. 2001b; 2:357–368. [PubMed: 11331910]

Van Veldhoven PP, Baes M. Peroxisome deficient invertebrate and vertebrate animal models. Front Physiol. 2013; 4:335. [PubMed: 24319432]

Wanders RJ. Metabolic functions of peroxisomes in health and disease. Biochimie. 2014; 98:36–44. [PubMed: 24012550]

Wanders RJ, Waterham HR. Peroxisomal disorders I: biochemistry and genetics of peroxisome biogenesis disorders. Clin Genet. 2005; 67:107–133. [PubMed: 15679822]

Wanders RJ, Waterham HR. Biochemistry of mammalian peroxisomes revisited. Annu Rev Biochem. 2006; 75:295–332. [PubMed: 16756494]

Warren DS, Morrell JC, Moser HW, Valle D, Gould SJ. Identification of PEX10, the gene defective in complementation group 7 of the peroxisome-biogenesis disorders. Am J Hum Genet. 1998; 63:347–359. [PubMed: 9683594]

Warren DS, Wolfe BD, Gould SJ. Phenotype-genotype relationships in PEX10-deficient peroxisome biogenesis disorder patients. Hum Mutat. 2000; 15:509–521. [PubMed: 10862081]

Webster HD, Martin R, O'Connell MF. The relationships between interphase Schwann cells and axons before myelination: a quantitative electron microscopic study. Dev Biol. 1973; 32:401–416. [PubMed: 4789698]

Williams C, van den Berg M, Geers E, Distel B. Pex10p functions as an E-3 ligase for the Ubc4p-dependent ubiquitination of Pex5p. Biochem Bioph Res Co. 2008; 374:620–624.

Williams C, van den Berg M, Panjikar S, Stanley WA, Distel B, Wilmanns M. Insights into ubiquitin-conjugating enzyme/ co-activator interactions from the structure of the Pex4p:Pex22p complex. EMBO J. 2012; 31:391–402. [PubMed: 22085930]

Zemski Berry KA, Murphy RC. Electrospray ionization tandem mass spectrometry of glycerophosphoethanolamine plasmalogen phospholipids. J Am Soc Mass Spectrom. 2004; 15:1499–1508. [PubMed: 15465363]

Highlights

- Mouse *Pex10* model displays progressive loss of movement during late embryogenesis.
- *Pex10*$^{CY/CY}$ embryos show phenotypic and biochemical hallmarks of PBD.
- *Pex10*$^{CY/CY}$ embryos display characteristic signs of defects in axon integrity.
- *Pex10*$^{CY/CY}$ embryos have misplaced Schwann Cells along axons and at synapses.
- *Pex10*$^{CY/CY}$ phrenic axons extend beyond defective synapses in muscle.

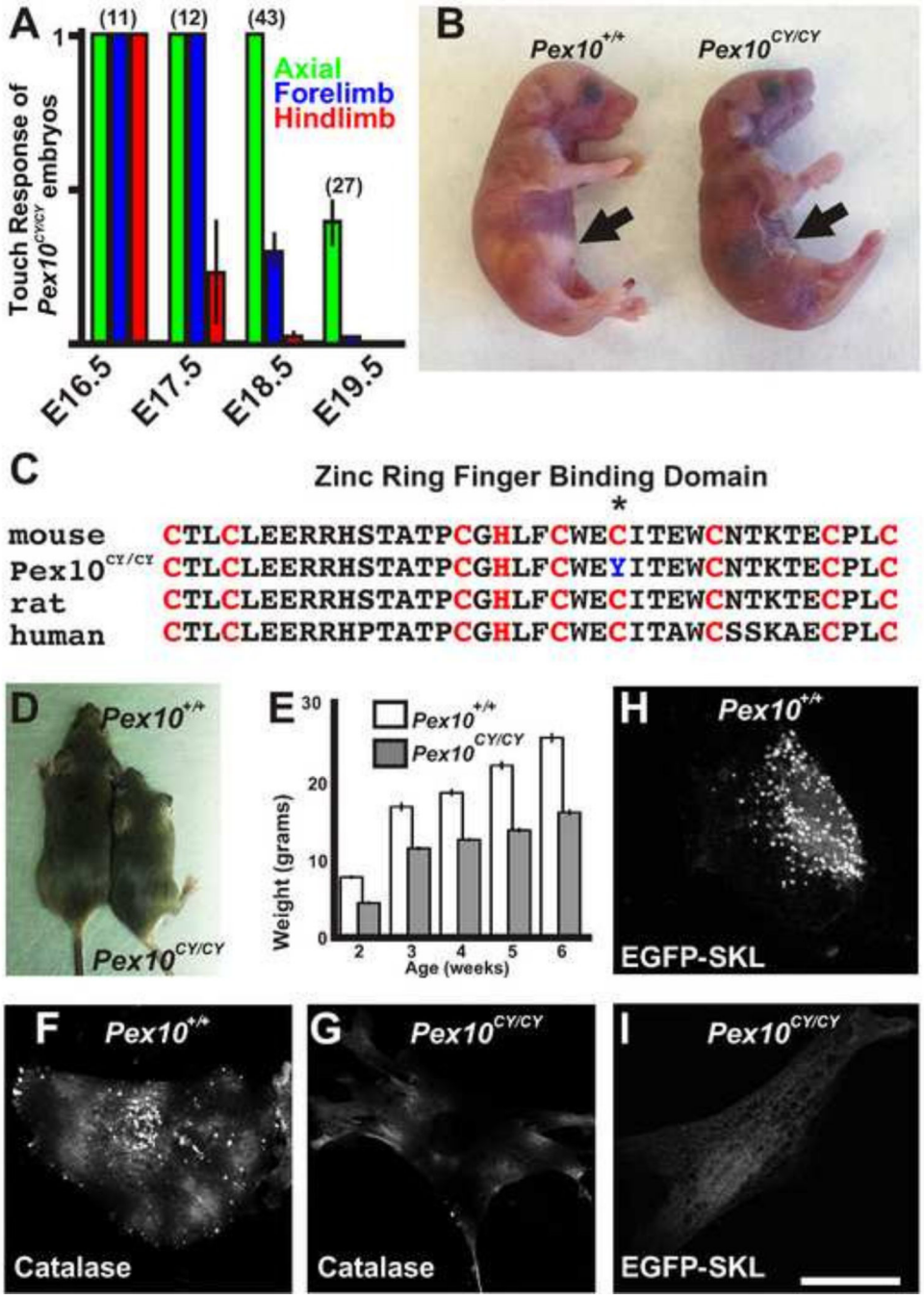

Figure 1. Identification of *Pex10*$^{CY/CY}$ mutants with defects in peroxisome function

A. Touch assay to examine movement during late stages of embryonic mouse development shows a progressive loss of locomotor movement in *Pex10*$^{CY/CY}$ mutants. B. Neonatal littermates within 2 hours of birth. *Pex10*$^{CY/CY}$ mice are cyanotic and show no milk in the stomach (black arrows). C. A cysteine in the conserved PEX10 zinc ring finger binding domain (red letters, C_3HC_4) is mutated in *Pex10*$^{CY/CY}$ mice (asterisk). D. Surviving *Pex10*$^{CY/CY}$ mouse (right) shown with wildtype littermate. E. Difference in weight between *Pex10*$^{CY/CY}$ mice (n=2) and wildtype littermates (n=3). F, G Antibodies to catalase label the

peroxisomes in wildtype embryonic fibroblast (F) but shows only diffuse cytoplasmic labeling in *Pex10*$^{CY/CY}$ MEFs (G). H, I Peroxisomal import signal EGFP-SKL is localized to peroxisomes in wildtype MEFs (H) but no punctate labeling is seen in *Pex10*$^{CY/CY}$ MEFs (I). Scale bar=50 μm.

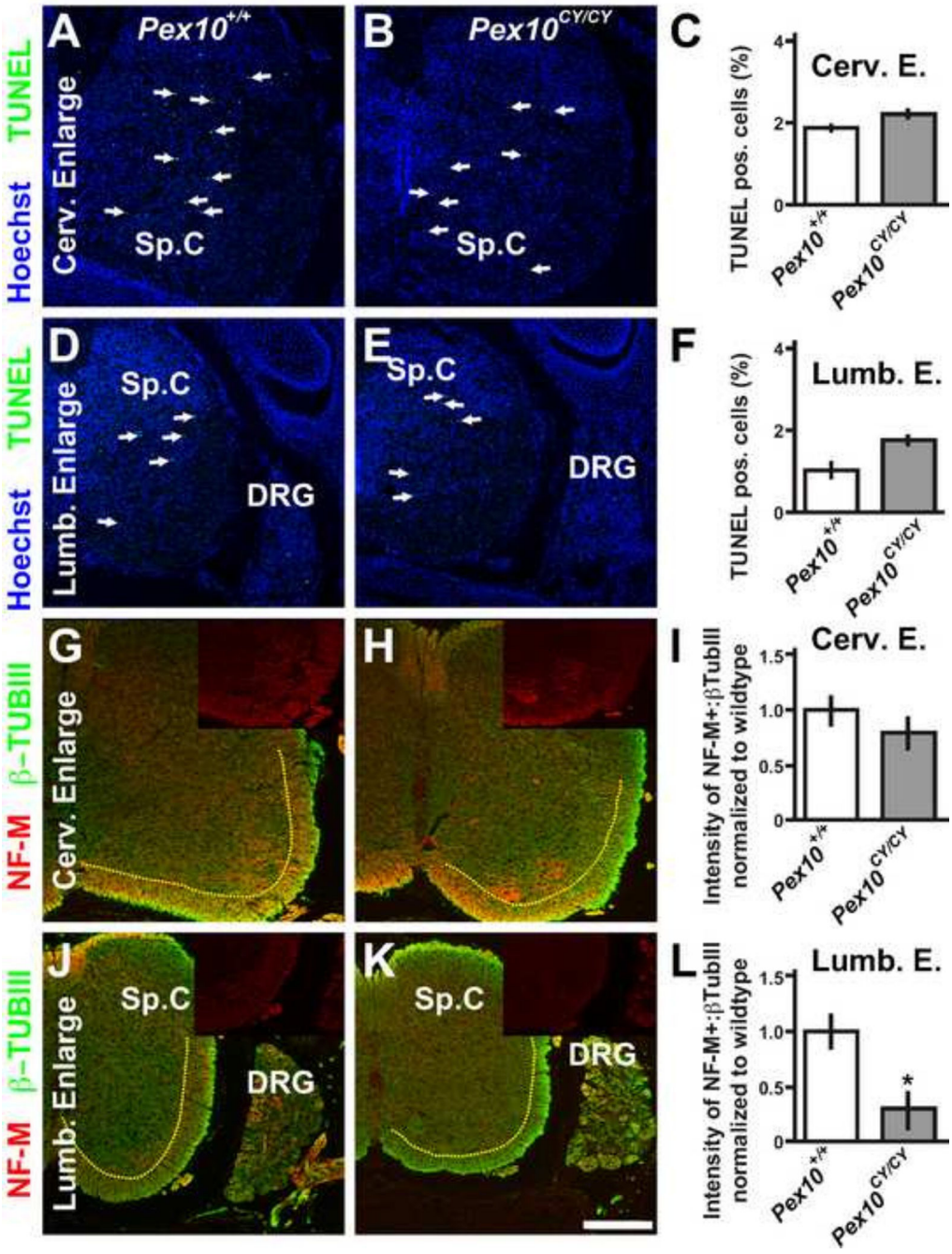

Figure 2. *Pex10*$^{CY/CY}$ spinal cords show defects in white matter axons

A–F. TUNEL labeling to detect apoptotic cells (green) in E18.5 wildtype (A, D) and *Pex10*$^{CY/CY}$ (B, E) spinal cord enlargements (the regions of the spinal cord that harbor limb innervating motoneurons) at cervical (A, B) and lumbar (D, E) levels (blue are nuclei stained with Hoechst 33342, white arrows identify TUNEL labeled cells). C, F. Quantification of TUNEL labeling/total nuclei shows no statistical difference in apoptosis between wildtype and *Pex10*$^{CY/CY}$ spinal cords or sensory neurons within the dorsal root ganglion (DRG), (n=16 sections from 3 embryos, average cells per slice ranged from 2996–

4552; Cervical level in wild type: 1.96+/− 0.08%, *Pex10*$^{CY/CY}$: 2.16+/−0.10%; p=0.39; Lumbar wild type: 1.04+/− 0.17%; *Pex10*$^{CY/CY}$: 1.81+/−0.11%; p=0.28; DRG cervical wildtype 0.36+/− 0.15%; *Pex10*$^{CY/CY}$ 0.27+/−0.11%; p=0.4; DRG lumbar wildtype 0.09+/− 0.08%; *Pex10*$^{CY/CY}$ 0.11+/−0.05%; p=0.32). G–L. Neurofilament (NF-M, red) and β-tubulin III (β-TubIII, green) label axons in spinal cord enlargements at cervical (G, H) and lumbar (J, K) levels (brightness level of β-TubIII was equally lowered on G, H, J, K to allow visualization of NF-M; insets show NF-M alone). I, L. Quantification of the ratio NF-M:β-TubIII intensity normalized to wildtype in white mater region of spinal cords (white matter region is to the right and below the yellow dashed line). Scale bar=200μm. Asterisk in L indicates a significant difference (p = 0.004; *t*-test).

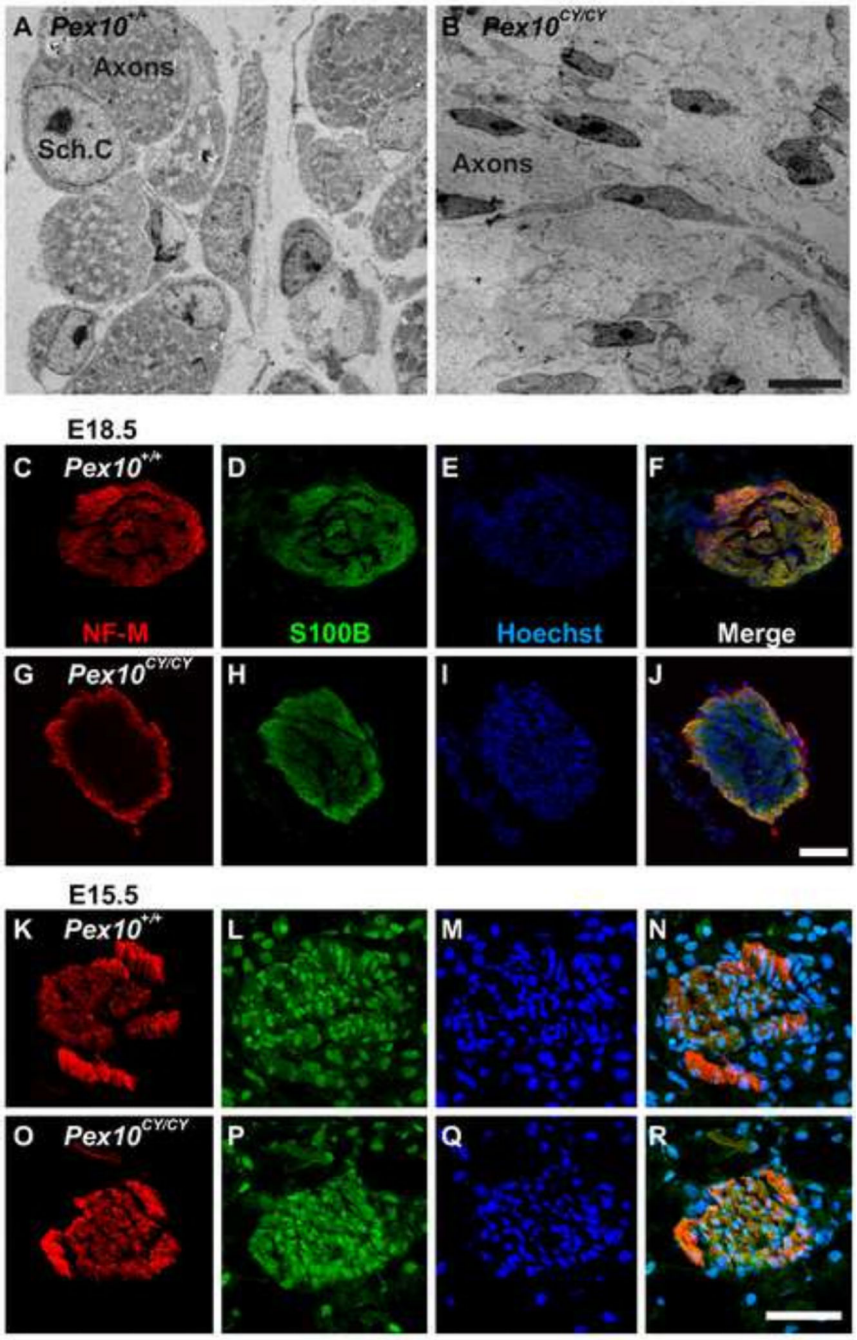

Figure 3. *Pex10*$^{CY/CY}$ sciatic nerves display Schwann cell and axon integrity defects

A, B. Isolated E18.5 wildtype and *Pex10*$^{CY/CY}$ sciatic nerves imaged by electron microscopy. A. Central region of sciatic nerve showing stereotypical encapsulation of axons bundles by early Schwann cells.. B. Similar region in *Pex10*$^{CY/CY}$ sciatic nerves shows defects in encapsulation of axons bundles and early Schwann cells are either absent or show abnormal morphology as elongated fibroblast-like cells. C–R. Labeling with antibodies to NF-M (axons, red), S100B (Schwann cells, green) and Hoechst 33342 (nuclei, blue) of E18.5 (C–J) and E15.5 (K–R) wildtype and *Pex10*$^{CY/CY}$ sciatic nerves. C–F. E18.5 wildtype

sciatic nerves show axon and Schwann cell labeling throughout the cross section. G–J. E18.5 *Pex10*$^{CY/CY}$ sciatic nerves have reduced labeling of axons and Schwann cells in the central region of sciatic nerve. K–R. E15.5 wildtype and *Pex10*$^{CY/CY}$ sciatic nerves from hindlimb cross sections have similar distribution of axon and Schwann cell labeling. A,B Scale bar=5μm. C–R Scale bar=50μm.

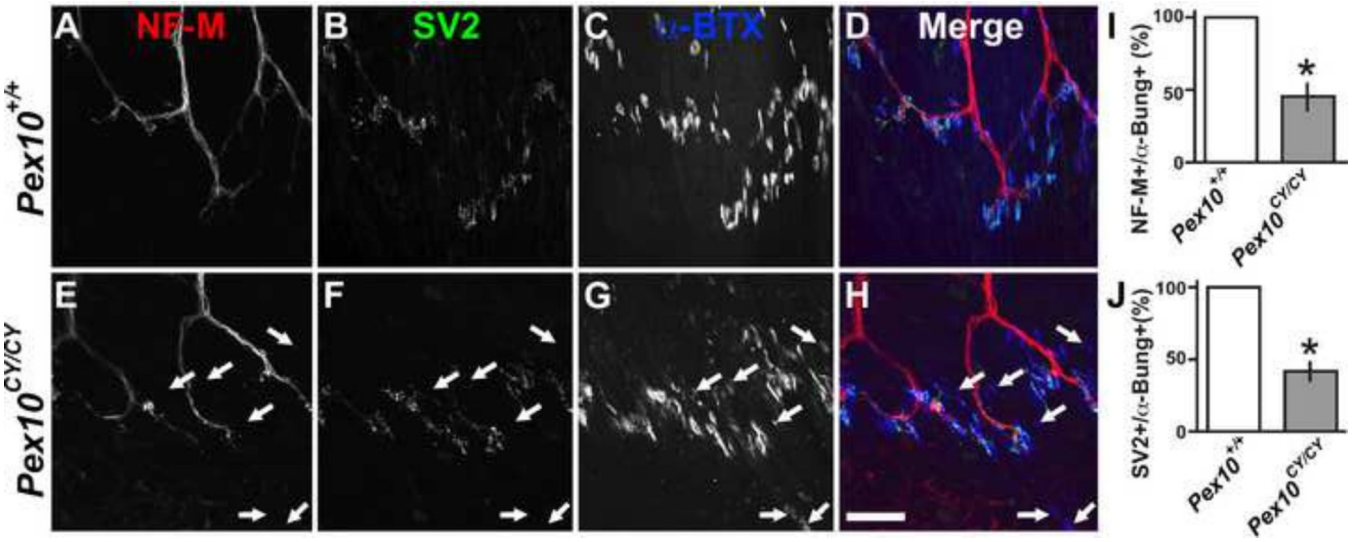

Figure 4. *Pex10*$^{CY/CY}$ soleus muscle exhibits NMJ defects

A–H. E18.5 soleus muscle from wildtype (A–D) and *Pex10*$^{CY/CY}$ (E–H) littermates labeled with NF-M (axons, red), SV2 (pre-synaptic vesicles, green) and α-BTX (post-synaptic AChR clusters, blue). A–D. Stereotypical pattern of innervation in wildtype soleus muscle with co-localization of pre- and post-synaptic apparatus. E–H. In *Pex10*$^{CY/CY}$ mutants there is not a strong correspondence between NF-M, SV2, and α-BTX labeling. I. Quantification of NF-M positive axons that are opposed to α-BTX+ AChR clusters. J. Quantification of SV2 positive vesicles adjacent to α-BTX+ AChR clusters. White arrows in E–H indicate α-BTX+ AChR clusters that lack SV2+ and NF-M+ co-labeling. Scale bar=50μm. Asterisks indicate a significant difference ($p < 0.005$; *t*-test).

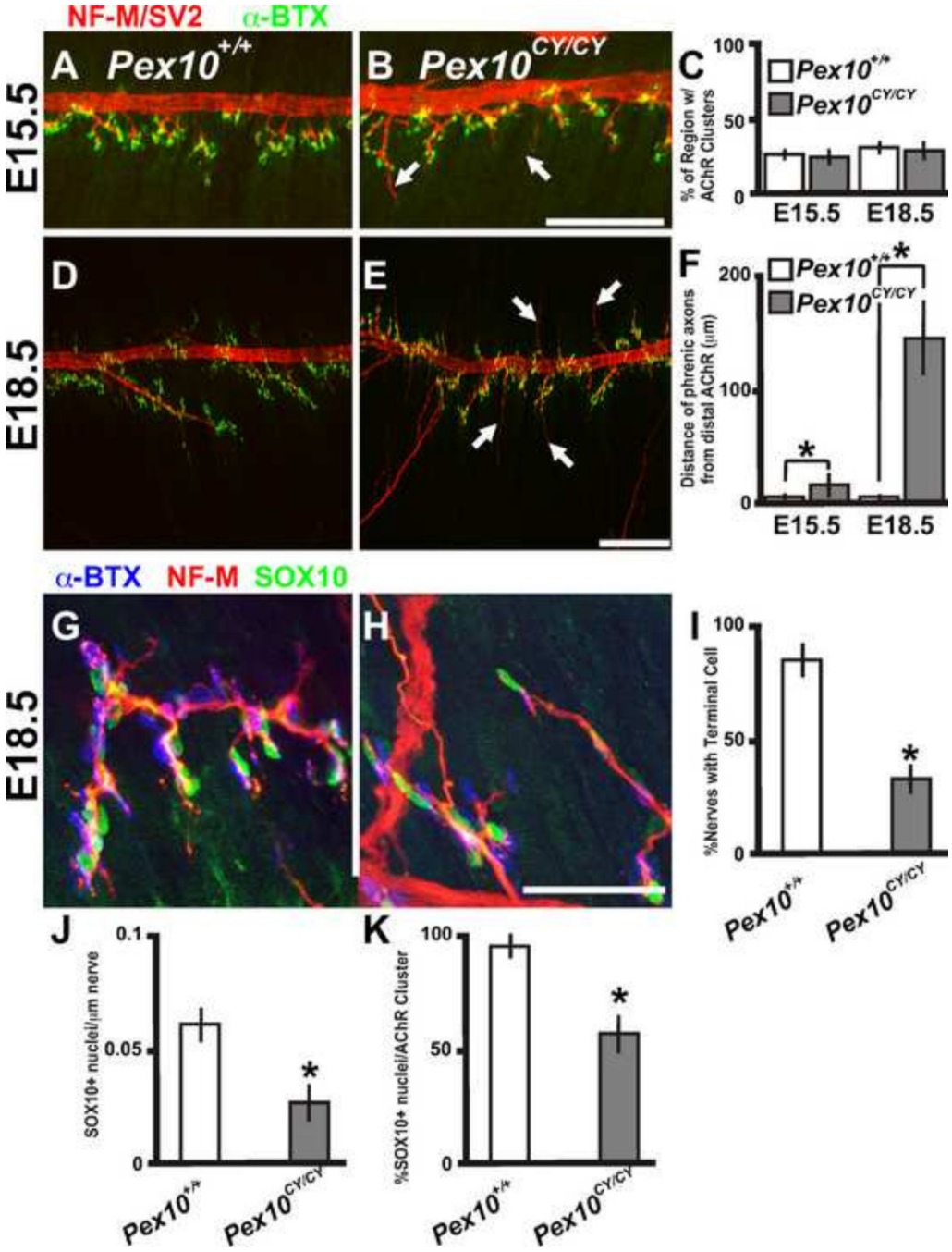

Figure 5. *Pex10*$^{CY/CY}$ diaphragms display defects in axon extension and Schwann cell placement

A, B, D, E. E15.5 (A, B) and E18.5 (D, E) wildtype and *Pex10*$^{CY/CY}$ diaphragms labeled with NF-M/SV2 (axons and pre-synaptic sites) and α-BTX (post-synaptic AChR clusters). C. Quantification as a percentage of the region of the diaphragm with AChR clusters in E15.5 and E18.5 wildtype and *Pex10*$^{CY/CY}$ diaphragms. F. Quantification of axon extension beyond the AChR clusters in E15.5 and E18.5 *Pex10*$^{CY/CY}$ diaphragms. G, H. E18.5 wildtype (G) and *Pex10*$^{CY/CY}$ (H) diaphragms labeled with NF-M (axons), α-BTX (post-synaptic AChR clusters) and SOX10 (Schwann cell nuclei, green). I. Quantification of

percentage of nerves with SOX10 positive nuclei at the terminal end of the nerve. J. Quantification of SOX10 positive nuclei along the length of the nerve. K. Quantification of SOX10 positive nuclei adjacent to AChR clusters. A, B, D, E. Scale bar=200μm. G-H Scale bar=50μm. Asterisks indicate a significant difference ($p < 0.005$; *t*-test).

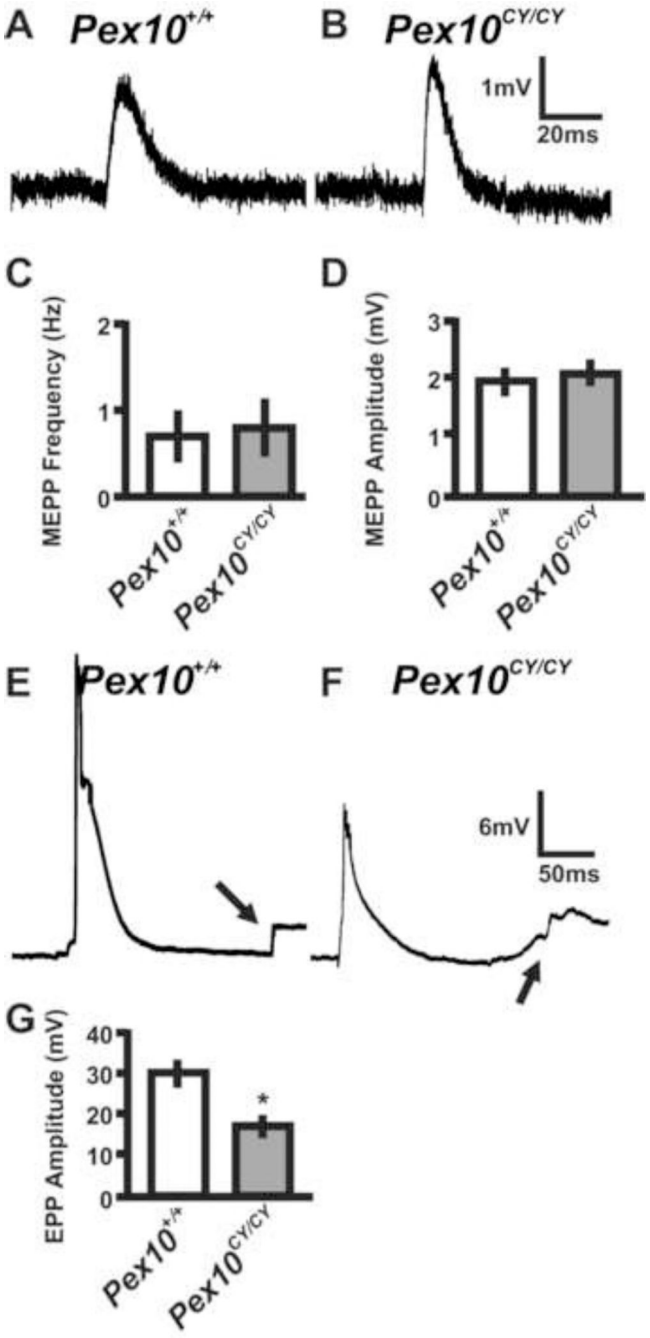

Figure 6. *Pex10*$^{CY/CY}$ diaphragm muscle displays decreased evoked transmitter release

Sharp electrode recordings of E18.5 wildtype and *Pex10*$^{CY/CY}$ diaphragms in Ringer's solution. A, B. Representative spontaneous EPP (MEPP) from E18.5 wildtype and *Pex10*$^{CY/CY}$ diaphragms. C, D. Quantification of MEPP frequency and amplitude. E, F. Representative evoked EPP from E18.5 wildtype and *Pex10*$^{CY/CY}$ diaphragms (Note; arrows highlight the muscle contraction after the EPP). G. Quantification of EPP amplitude. Scale

bars adjacent to traces in B and F. Asterisk in G indicates a significant difference (p= 0.001; *t*-test).

Table 1

Biochemical analysis of human and mouse bloodspots

	Mice E18.5	**E18.5**	**E18.5**	**Mice Adult**	**Adult**	**Adult**	**Human Samples**		
	***Pex10*$^{+/+}$ n=10**	***Pex10*$^{CY/+}$ n=4**	***Pex10*$^{CY/CY}$ n=8**	***Pex10*$^{+/+}$ n=6**	***Pex10*$^{CY/+}$ n=6**	***Pex10*$^{CY/CY}$ n=2**	**Normal n=190**	**PBD n=62**	**RCDP n=9**
Total PE plasmalogen	13.33+/−9.7	4.41+/−0.38*	0.61+/−0.11*	7.19+/−1.06	16.48+/−9.21	6.05+/−5.15	64.18+/−40.30	26.66+/−30.28	10.72+/−12.07
C26:0-LPC%	0.30+/−0.15	0.47+/−0.06	3.60+/−1.75*	0.29+/−0.08	0.16+/−0.02	0.17+/−0.09	0.21+/−0.10	6.04+/−3.47	0.52+/−0.04
DHCA	0.05+/−0.04	0.04+/−0.03	0.61+/−0.18*	0.02+/−0.02	0.10+/−0.03	0.16+/−0.00	0.02+/−0.02	24.06+/−29.95	1.14+/−3.13
THCA	0.01+/−0.01	0.38+/−0.21*	0.39+/−0.06*	0.03+/−0.02	0.52+/−0.13*	1.03+/−0.09	0.03+/−0.02	13.12+/−24.96	0.35+/−1.10

Average value from bloodspots (see methods), Surviving adult *Pex10*$^{CY/CY}$ shows calculated median. Heterozygous adults were birthing females that produced phenotypic neonatal mice. PBD are patients with Peroxisomal Biogenesis Disorder. RCDP are patients with rhizomelic chondrodysplasia punctacta (due to mutation in PEX7).

Abbreviations: PE= ethanolamine phospholipids, DHCA= dehydrocholic acid, THCA= 3 alpha, 7 alpha, 12 alpha-Trihydroxy-5 beta-cholestan-26-oic acid, LPC=lysophosphocholines. Asterisks indicates significance by t-test $p<0.005$ while values are +/− SD